Object Characterization Based on Multispectral Acoustic Imaging

Xinhua Guo, Yosuke Mizuno, and Kentaro Nakamura

Precision and Intelligence Laboratory, Tokyo Institute of Technology, Yokohama 226-8503, Japan
E-mail: guoxinhua@sonic.pi.titech.ac.jp

In previous studies, acoustic imaging was conducted using a single frequency or a limited number of frequencies that were not sufficient to clearly describe and explain the object characteristics. In this study, multispectral acoustic imaging (MSAI) is proposed to reveal rich information of object characteristics. An experimental study on object surfaces is conducted to verify the validity of the technique. Acoustic imaging of object surfaces is performed on the basis of a significant number of spectra over a wide frequency range. Using the frequency-swept irradiation from 1 to 20 kHz at 30 Hz intervals, we demonstrate the visualization of the following three different object surfaces: a rigid surface with small holes with and without a piece of thin paper covering the surface, and a boundary between wood and rubber plates. The distributions of sound pressure reconstructed at each frequency by a near-field acoustic holography (NAH) technique are shown. In multispectral acoustic imaging, frequency dependence provides us rich information about the surface shape and material properties of the objects; thus, the characteristics of the surfaces are successfully visualized. © 2013 The Japan Society of Applied Physics

1. Introduction

Since acoustic waves travel into materials in which electromagnetic waves do not propagate, visualizations in water, the human body, and solid objects have been carried out using acoustic waves. Typical successful examples include underwater sound navigation and ranging (SONAR),[1–3] medical ultrasonic echography,[4,5] and non-destructive evaluation.[6,7] In these visualization techniques, the target object is irradiated with acoustic waves, and the reflected or transmitted waves are observed. Acoustically obtained images provide different information from optical images, and are greatly affected by the elastic properties and surface structures of the object. These are reflected in the frequency responses since frequency-dependent phenomena, such as resonance, diffraction, and attenuation are essentially related to the properties of the object. Consequently, frequency band width is important in acoustic imaging for obtaining more highly functional information. In optical observations, recently the use of a multispectral camera[8,9] has been spreading in studies on remote sensing and medical tissue diagnostics. As an analogy to the multispectral imaging in optics, a few studies on acoustics have been reported, but only a single frequency or a limited number of frequencies were used in such conventional acoustic imaging.[10]

We demonstrate, in this study, acoustic imaging utilizing a wide frequency band with a fine frequency step, which is called multispectral acoustic imaging (MSAI). Images are obtained for one object at a large number of frequencies, and analysis of the relationship between the multispectral acoustic images and the physical properties of the object is carried out. In this paper, first, the experimental setup is explained. Next, the image reconstruction technique based on near-field acoustic holography (NAH) is briefly reviewed, which is used to reconstruct the images on the object surface from the sound pressure distribution measured on a plane located near the object surface. Finally, demonstrations on the following three surfaces are carried out to verify the feasibility and usefulness of MSAI in practice: (i) a rigid surface with drilled holes with different diameters and depths, (ii) a drilled surface covered by a piece of thin paper, and (iii) a boundary between two different materials.
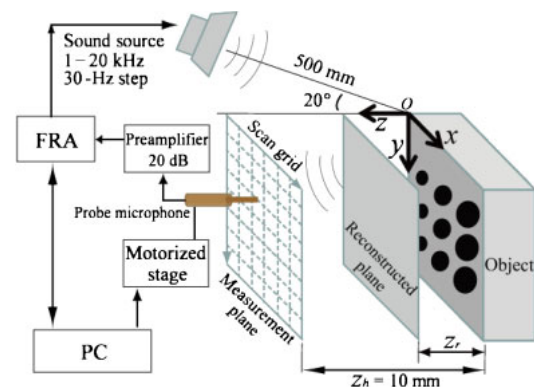

Fig. 1. (Color online) Experimental setup.

2. Experimental Methods

The complex sound pressure as a combination of amplitude and phase information was measured at the hologram plane (measurement plane) using the experimental setup shown in Fig. 1. The object was irradiated with frequency-swept sound from 1 to 20 kHz emitted from a small loudspeaker (Fostex T90A). The loudspeaker had a frequency response from 5 to 35 kHz that did not affect the experimental results, since the normalization was carried out at each frequency to generate an image. The sound pressure at the measurement plane was in the range from 90 to 115 dB. The distance between the sound source and the object was 500 mm, and the incident angle was 20°. A needle microphone (B&K 4182) was scanned two-dimensionally over a plane near the object using a motorized stage. The microphone had an almost constant sensitivity of 3.16 mV/Pa in the frequency range from 1 Hz to 20 kHz. The X–Y scanning area was determined depending on the dimensions of the object surface. The received signal was processed using a frequency response analyzer (FRA; NF5097), and the amplitude and phase at each frequency were sent to a personal computer (PC) for further processing. The reconstructed images ($z_r = 0$ mm) were obtained on the object surface by NAH. The distance between the measurement plane (z_h) and the object surface was 10 mm throughout the experiments.
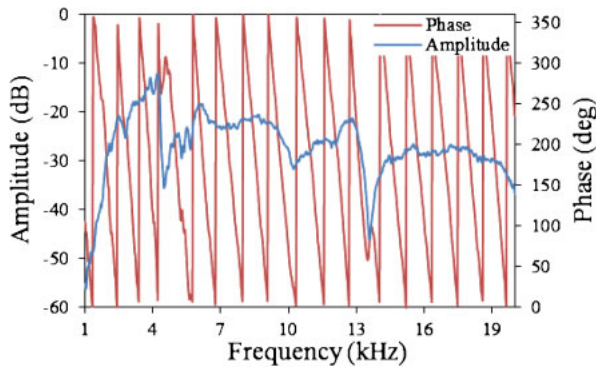
Fig. 2. (Color online) Example of frequency response.

3. Data Acquisition and Signal Processing

3.1 Data acquisition for the complex sound pressure

The signal driving the loudspeaker was generated by the FRA, and was used as the reference signal for determining the phase of the sound pressure measured using the microphone. The frequency responses from 1 to 20 kHz at 30 Hz intervals were recorded for all the scanning positions. Figure 2 shows one of the typical recorded data (for the object of the first demonstration) of amplitude and phase just on a point located at the center of the hole of 4 mm in diameter and 20 mm in depth. The amplitude was displayed as a relative value, where 0 dB is equal to the sound pressure of 144 dB. This frequency-swept measurement was repeated at every scanning point. After the measurement was finished, the acquired data were arranged into two-dimensional distributions of the amplitude and phase at each frequency, as shown in Fig. 3, which means that we have acoustic holograms from 1 to 20 kHz at 30 Hz intervals. The total number of holograms obtained was 635.

3.2 Reconstruction of sound pressure distribution based on NAH

To visualize the characteristics of object surfaces, the planar NAH[11,12] was applied to the measured sound pressure. Here, let us briefly review the procedure that we employed. The fundamental equation for the pressure distribution on the surface is derived from the Rayleigh integral equation[13]

$$p_r(x, y, z)$$
$$= \int_{-\infty}^{\infty} \int_{-\infty}^{\infty} p_h(x_h, y_h, z_h) g_D(x - x_h, y - y_h, z - z_h) \, dx_h \, dy_h, \tag{1}$$

where $p_r(x, y, z)$ is the complex acoustic pressure at a point (x, y, z) on the reconstruction plane, $p_h(x_h, y_h, z_h)$ is the complex acoustic pressure at a point (x_h, y_h, z_h) on the hologram plane, and g_D is the Dirichlet Green's function that acts as the transfer function of the sound pressure field from one point to another. The expression of two-dimensional Fourier transforms[13] is employed to express the sound field in the k-space:

$$\tilde{F}(k_x, k_y) = \int_{-\infty}^{\infty} \int_{-\infty}^{\infty} f(x, y) e^{-i(k_x x + k_y y)} \, dx \, dy \equiv F[f(x, y)], \tag{2}$$
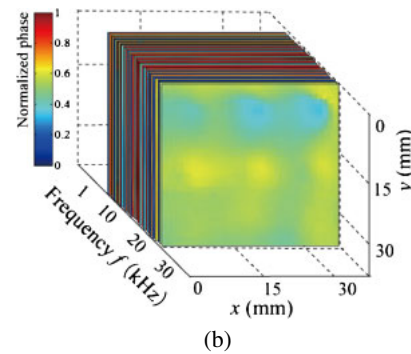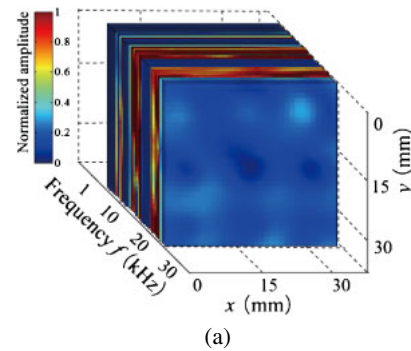

(a)

(b)

Fig. 3. (Color online) Distributions of the amplitude and phase in the whole frequency range: (a) amplitude and (b) phase distributions.

where (k_x, k_y) refers to the k-space, and (x, y) refers to the real space. Since Eq. (1) is expressed as a two-dimensional convolution integral of $p_h(x_h, y_h, z_h)$ and $g_D(x - x_h, y - y_h, z - z_h)$, being based on the convolution theorem,[14,15] Eq. (1) yields

$$p_r(x, y, z) = F^-[\tilde{P}_r(k_x, k_y, z)]$$
$$= F^-[\tilde{P}_h(k_x, k_y, z_h)\tilde{G}_D(k_x, k_y, z)], \tag{3}$$

where F^- indicates the inverse Fourier transform. This gives the holographic reconstruction of the sound pressure in the three-dimensional space $p_r(x, y, z)$ in terms of the Fourier transformed form $\tilde{P}_h(k_x, k_y, z_h)$ derived from the hologram data $p_h(x_h, y_h, z_h)$. The operator $\tilde{G}_D(k_x, k_y, z)$, that is, the two-dimensional spatial Fourier transform of the Dirichlet Green's function, is given as

$$\tilde{G}_D(k_x, k_y, z) = \begin{cases} \exp\left(iz\sqrt{k^2 - k_x^2 - k_y^2}\right) & k_x^2 + k_y^2 \leq k^2 \\ \exp\left(-z\sqrt{k_x^2 + k_y^2 - k^2}\right) & k_x^2 + k_y^2 > k^2 \end{cases}. \tag{4}$$

The pressure field in k-space is divided into two types of wave by the radiation circle represented by $k_x^2 + k_y^2 = k^2$. An evanescent wave exists inside the circle, while the propagating wave exists in the rest of the area.

4. Experimental Results

As mentioned in Sect. 1, acoustic images were easily influenced by the shape, size, structure, and material property of the objects. Three examples will be demonstrated in this paper. The first two examples exhibit clear resonances related to the structure. The resonant frequencies of a cylindrical cavity were studied by Harris et al.,[16] and are given as

$$f_{mn} = \frac{c}{2}\sqrt{\left(\frac{A}{d}\right)^2 + \left(\frac{\alpha_{mn}}{r_0}\right)^2}, \tag{5}$$
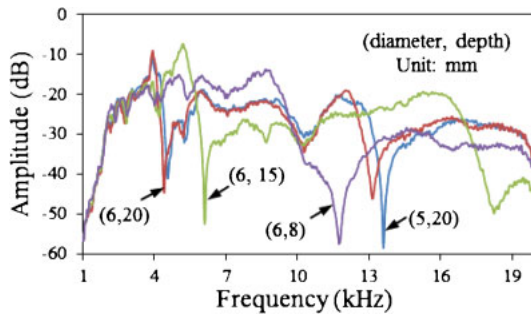
Fig. 4. (Color online) Frequency responses under four different conditions: diameter and depth.

where c is the sound speed in air, and d and r_0 represent the depth and radius of the cylindrical cavity, respectively. A denotes the integer number $(0, 1, 2, 3, \ldots)$, and the coefficient α_{mn} is the n-th solution of the equation $J'_m(\pi r) = 0$; here, J_m is the m-th order cylindrical Bessel function. The resonance frequency is related to the depth d and radius r of the cylindrical cavity.

In this experiment, the holes that were closed at one end and open at the other end were excited by acoustic incident waves. Here, a simple case was considered, where only the depth modes were excited. Then, the resonance frequencies are expressed as[17]

$$f_0 = \frac{Bc}{4d}, \quad B = 1, 3, 5, 7, \ldots. \quad (6)$$

4.1 Demonstration 1: Surface profile

The sample for the first demonstration was a resin block with 9 holes of different diameters (4, 5, and 6 mm) and depths (8, 15, and 20 mm) on one surface, as shown in Fig. 5(a). The scanning area for the microphone was $33 \times 33\,\mathrm{mm}^2$ near the object surface, and the grid spacing of the scanned area was $1 \times 1\,\mathrm{mm}^2$.

4.1.1 Basic frequency responses

To explain the typical results, frequency responses at four measurement points for the different holes were extracted from all the measured points on the surface, and are shown in Fig. 4. The fundamental and second-order resonances for each hole were observed except for the hole of 8 mm in depth. The responses to the different depths of 8, 15, and 20 mm exhibited different frequency dependences since the holes had acoustic resonances characterized by the depth. The lower cutoff frequency of the loudspeaker is 3.6 kHz, and may result in the slope observed from 1 to 3 kHz in Fig. 4.

According to Eq. (6), which represents the resonant case of a one-dimensional closed-end pipe resonating at the odd harmonics, i.e., $\lambda/4$, $3\lambda/4$, $5\lambda/4$, and $7\lambda/4, \ldots$ (λ is the sound wavelength), the resonance frequency of each hole can be calculated to be 4250, 5667, and 10625 Hz, corresponding to the depths of 20, 15, and 8 mm, respectively. From Fig. 4, the measured resonant frequencies were 4390, 6100, and 11680 Hz. Compared with the calculated and measured values, although open-end correction should be required for precise discussion, the depths of the holes were identified by the frequency. On the other hand, even

when the depth was the same ($= 20\,\mathrm{mm}$), the holes with different diameters (5 and 6 mm) showed different frequency responses, which demonstrates that the diameter has some effects on the frequency responses.

4.1.2 Images at every frequency

All of the 635 holograms from 1 to 20 kHz at a 30 Hz step were reconstructed using the discrete form of the Rayleigh integral in Eq. (3). Five reconstructed images in three-dimensional form of the object picked up from the whole range of frequencies are shown in Figs. 5(b)–5(f). With increasing frequency, the holes at each line and column showed different responses since the holes had acoustic resonances characterized by the depth: the deepest holes had the responses at lower frequencies, as shown in Fig. 5(b). The holes at the second and third lines are observed in Figs. 5(c) and 5(e). The diameter had some effects on the frequency responses. The holes of the second line with different diameters were not observed simultaneously although the holes had the same depth, as shown in Fig. 5(d). Although it was difficult to identify the holes with the same diameters from optical images, depth information was easily obtained by the multispectral acoustic imaging technique. The holes at each column were not observed at the same time except for the higher harmonics, as shown in Fig. 5(f). In addition to the holes at the third line, the response of the second harmonic was observed in the first line.

The holes of the first line were observed in the band from 3.5 to 5.5 kHz, since they had the same depth and different diameters, but the different diameters had some effects on the frequency responses so that there was a slight fluctuation in a certain frequency range. For example, the two holes $(5, 20)$ and $(6, 20)$ had closed resonance frequencies, as shown in Fig. 4. From 5.5 to 7.5 kHz, responses were found in the second line, and the band from 10.5 to 14.0 kHz for the last line. From these results, the detailed structures of the object seem to correspond to their characteristic acoustic spectral bands.

4.2 Demonstration 2: Surface covered by paper

In the second experiment, the surface of the sample used in Fig. 5(a) was covered with a piece of paper, as shown in Fig. 6(a). The thickness of the paper was approximately 0.1 mm. Acoustic responses were, however, still observed, although the holes can hardly be seen optically, which indicates that the buried structures can be identified under a certain condition. The acoustic images at the specific frequencies where the holes at the first, second, and third lines were recognized are shown in Figs. 6(b)–6(d), respectively. Compared with the results in Figs. 5(b), 5(c), and 5(e), corresponding to the three frequencies of 4780, 6280, and 12220 Hz, respectively, the paper had almost no effect on the reconstructed images, i.e., the holes were visualized at nearly the same frequencies as in the experiments without the paper. The magnitude of the responses was almost unchanged in the case of employing the paper.

4.3 Demonstration 3: Material properties of the surfaces

The last experiment was carried out to investigate the effects of the material properties on the result of MSAI. The sample with a boundary between two regions with different reflec-
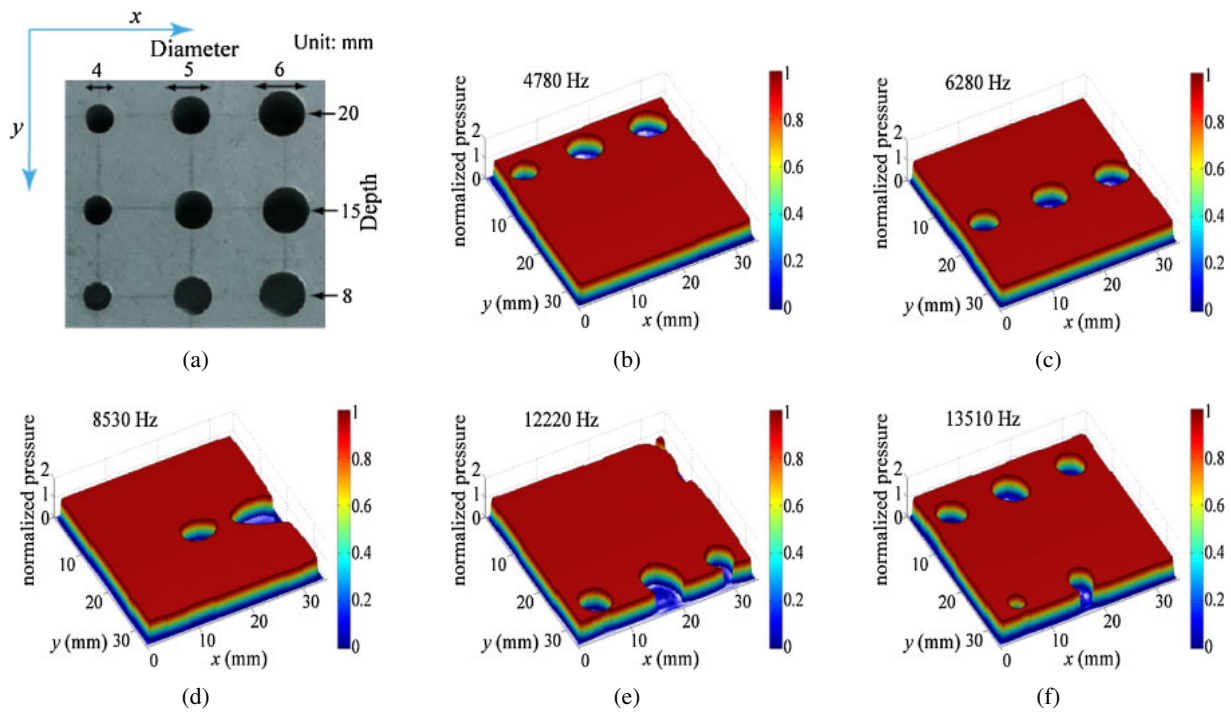
Fig. 5. (Color online) (a) Optical image and (b)–(f) reconstructed images at different frequencies of the object surface.
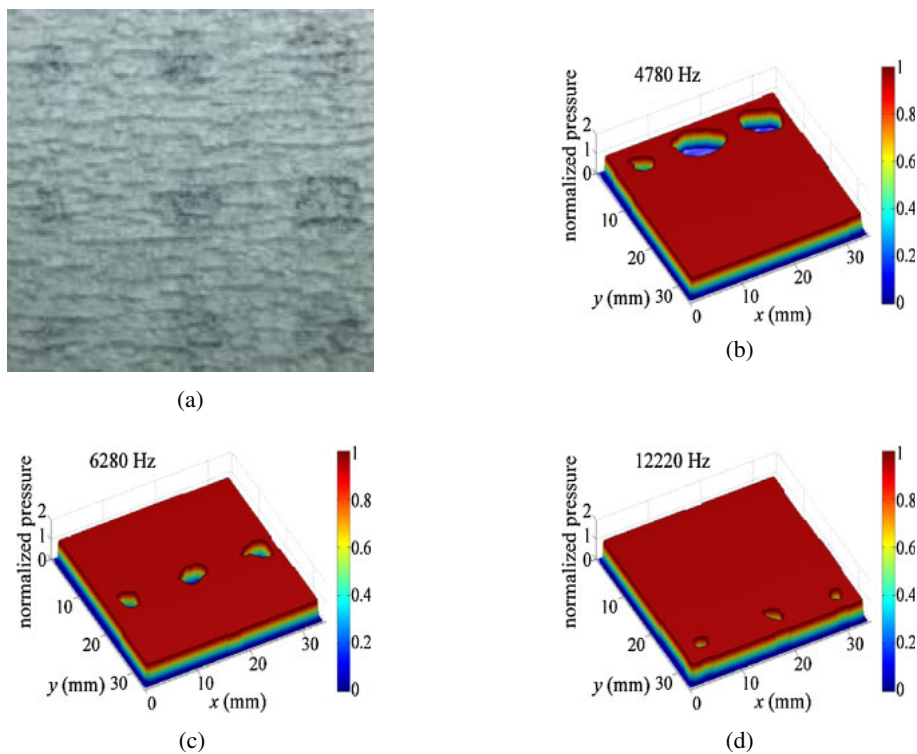

Fig. 6. (Color online) (a) Optical image and (b)–(d) reconstructed images at different frequencies with the holes covered by a piece of paper.

tivities is shown in Fig. 7(a). The upper part of the sample was a rubber plate, and the lower part was a wood plate. The acoustic impedances of the rubber and wood plates were approximately 12000 and 1148000 Pa·s/m, respectively. The original size of the object surface was 100×100 mm^2, and the measurement area was 50×50 mm^2 located at the center of the sample. The spatial interval between two scanning points was 2 mm. The same measurement as the previous

two experiments was carried out on this sample. Five images of the 635 reconstructed sound pressures were picked up, as shown in Figs. 7(b)–7(f). The red color represents the maximum magnitude, while the blue color denotes the minimum magnitude.

Figures 7(b) and 7(e) show the images of the reconstructed sound pressure on the surfaces at 3550 and 12790 Hz, respectively. The reconstructed sound pressure on the two plates
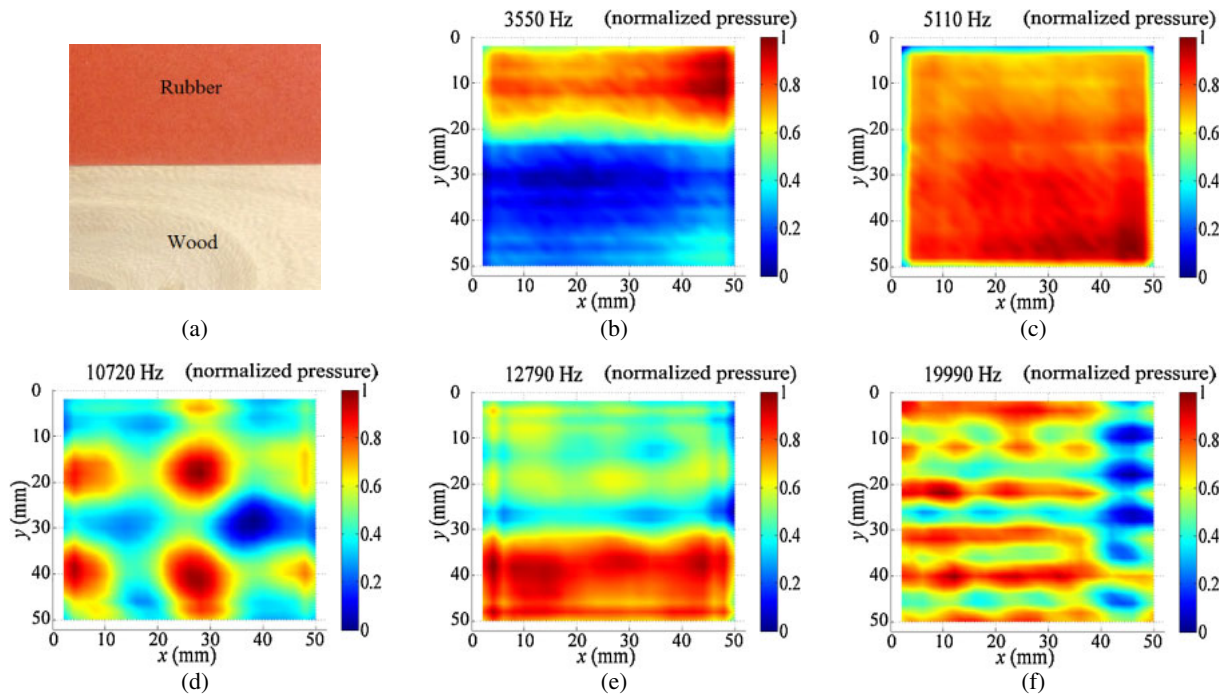
Fig. 7. (Color online) (a) Optical image and (b)–(f) distributions of sound pressure on two surfaces composed of different materials.

was different. The reconstructed sound pressure on the rubber plate was larger than that on the wood plate at a frequency of 3550 Hz, while that on the wood plate was larger than that on the rubber plate at a frequency of 12790 Hz.

In Figs. 7(c), 7(d), and 7(f), no obvious boundary was observed between the two surfaces, and thus at some frequencies, it was difficult to identify the two surfaces composed of different materials. At a frequency of 5110 Hz, the reconstructed sound pressure of the two surfaces was distributed almost uniformly, as shown in Fig. 7(c). Fringe patterns were observed at frequencies of 10720 and 19990 Hz, which might be affected by the interference between the irradiated sound and the reflected one. Thus, the material properties of the object surfaces can be identified by observation at many frequencies, although they cannot be found by using only one or few frequencies.

5. Conclusions

We reported the first trial to demonstrate the effectiveness of the multispectral acoustic imaging. Acoustic images were recorded from 1 to 20 kHz at 30 Hz intervals for three demonstrations. The results showed that the different structures of the surface and material properties of the objects were identified or recognized if the frequency responses were observed for a wide frequency range with fine pitch. The present approach might be an analogy to a multispectral camera in optics, which has recently been used for characterization in various applications instead of the conventional red, green, and blue (RGB) camera. The multispectral imaging is easily accomplished in acoustics, and powerful processing methods such as acoustic holography and other imaging techniques can enhance the usefulness of MSAI.

The large number of measurement points required a long time to complete the data acquisition. For high-speed measurement, a large-scale microphone array and a smart data acquisition system are required. For more precise characterization, the evaluation of the illuminating sound source such as the uniformity of the strength in space and frequency needs to be studied. MSAI provides a large volume of data, and it is difficult to display them in one image. We also investigated how to display the MSAI data using an RGB representation method.[18]

1) R. H. Wallace, H. V. Hillery, G. R. Barnard, B. M. Marks, and C. M. McKinney: J. Acoust. Soc. Am. **57** (1975) 862.
2) M. Palmese and A. Trucco: IEEE J. Oceanic Eng. **35** (2010) 584.
3) T. Tanaka, Y. Hama, H. Shiba, and I. Yamaguchi: Jpn. J. Appl. Phys. **42** (2003) 3225.
4) R. E. Apfel: Br. J. Cancer **45** (1982) 140.
5) A. Matani, Y. Ban, O. Oshiro, and K. Chihara: Jpn. J. Appl. Phys. **35** (1996) 3121.
6) R. Nakase, K. Nakata, and M. Matsukawa: Jpn. J. Appl. Phys. **51** (2012) 07GB16.
7) D. Shiraishi, R. Kato, H. Endoh, and T. Hoshimiya: Jpn. J. Appl. Phys. **49** (2010) 07HB13.
8) F. Feyaerts and L. van Gool: Pattern Recognition Lett. **22** (2001) 667.
9) R. Lu: Postharvest Biol. Technol. **31** (2004) 147.
10) N. Yoshizumi, S. Saito, D. Koyama, K. Nakamura, A. Ohya, and I. Akiyama: J. Med. Ultrason. **36** (2009) 53.
11) J. D. Maynard, E. G. Williams, and Y. Lee: J. Acoust. Soc. Am. **78** (1985) 1395.
12) W. A. Veronesi and J. D. Maynard: J. Acoust. Soc. Am. **81** (1987) 1307.
13) E. G. Williams: *Fourier Acoustics — Sound Radiation and Nearfield Acoustical Holography* (Academic Press, San Diego, CA, 1999) p. 31.
14) J. W. Goodman: *Introduction Fourier Optics* (McGraw-Hill, New York, 1968) p. 10.
15) E. G. Williams: *Fourier Acoustics — Sound Radiation and Nearfield Acoustical Holography* (Academic Press, San Diego, CA, 1999) p. 3.
16) J. M. Harris, D.-L. Xu, X.-M. Wang, Y.-J. Song, J.-S. Cong, and D.-H. Hen: Chin. J. Geophys. **48** (2005) 493.
17) M. L. Pollack: J. Acoust. Soc. Am. **67** (1980) 1153.
18) X. Guo, Y. Wada, Y. Mizuno, and K. Nakamura: Meas. Sci. Technol. **24** (2013) 105401.